ELSEVIER

Tactical hybrids of Li^+-conductive dry polymer electrolytes with sulfide solid electrolytes: Toward practical all-solid-state batteries with wider temperature operability

Dae Yang Oh [1], Kyu Tae Kim [1], Sung Hoo Jung [1], Dong Hyeon Kim [1], Seunggoo Jun [1], Sungeun Jeoung [2], Hoi Ri Moon [2], Yoon Seok Jung [1,*]

[1] Department of Chemical and Biomolecular Engineering, Yonsei University, Seoul 03722, South Korea
[2] Department of Chemistry, Ulsan National Institute of Science and Technology, Ulsan 44919, South Korea

The chemical vulnerability of sulfide solid electrolyte (SE) materials to organic polar solvents complicates the wet-slurry fabrication of sheet-type electrodes and SE films for practical all-solid-state Li batteries (ASLBs). Moreover, the disruption of interfacial Li^+ conduction by binders is problematic. This could be relieved by blending with liquid electrolytes but at the expense of the ASLBs' thermal stability. In this study, a new tactical approach to hybridize sulfide SEs with thermally stable and slurry-fabricable dry polymer electrolyte (DPE)-type binders is reported. Along with their practicability, ester solvents bearing bulky hydrocarbons, such as benzyl acetate, dissolve both polymers and Li salts (e.g., LiTFSI) while undamaging sulfide SEs. The use of the DPE-type binder, NA-LiTFSI (NA: nitrile butadiene rubber-poly(1,4-butylene adipate)), for $LiNi_{0.70}Co_{0.15}Mn_{0.15}O_2$ (NCM) electrodes significantly improves their electrochemical performance at 30 °C. Moreover, NA-LiTFSI is highly functional at 70 °C (from 180 to 200 mA h g^{-1} and from 84.2 to 91.8% for initial Coulombic efficiency) and applicable for other electrodes, such as graphite (from 265 to 330 mA h g^{-1}) and $Li_4Ti_5O_{12}$, which is in stark contrast to the solvate ionic liquid-type binder Li(G3)TFSI. Finally, pouch-type NCM/graphite ASLBs employing electrodes made of NA-LiTFSI binders were also fabricated.

Introduction

The solidification of electrolytes using inorganic materials for lithium or lithium-ion batteries (LIBs, all abbreviations are listed in Table S1) holds great promise of breakthroughs in enhanced safety and energy density [1–15]. In particular, mechanically deformable sulfide solid electrolyte (SE) materials could be integrated into composite electrodes by a simple cold-pressing process, thereby avoiding the fault-prone high-temperature sintering process [16–21]. Moreover, the Li^+ conductivities of these state-of-the-art candidate materials have reached ~10 mS cm^{-1} (e.g., $Li_{9.54}Si_{1.74}P_{1.44}S_{11.7}Cl_{0.3}$: [1] 25 mS cm^{-1} and $Li_{5.5}PS_{4.5}Cl_{1.5}$: [22,23] 12 mS cm^{-1}), this being equivalent to that of conventional organic liquid electrolytes [24]. However, their chemical sensitivity with regard to common organic solvents, such as N-methyl pyrrolidone (NMP), has posed an insurmountable obstacle to the industrial mass production of all-solid-state lithium-ion or lithium batteries (ASLBs), for which large-format sheet-type electrodes and SE films are fabricated using "soft" polymeric binders [18,19,25–34].

The vulnerability of sulfide SEs to nucleophilic attack by the polar functional groups of common organic solvents severely restricts available slurry-processing solvents to non-polar or less-polar solvents such as xylene [17,18,35,36]. However, to date only a limited number of solvents has been investigated without any systematic measurements of reactivity [18,37–40]. Even though the recent development of a dry process using polytetrafluoroethylene binder indicates an alternative route [41,42],

* Corresponding author.
E-mail address: Jung, Y.S. (yoonsjung@yonsei.ac.kr)

 https://doi.org/10.1016/j.mattod.2021.01.006

the wet-slurry process would still be preferable as only a minimal alteration in the manufacturing infrastructure for the transition from conventional LIBs to ASLBs would be required.

Hybridization with polymeric binders for practical ASLBs is imperative owing to their positive effects of releasing mechanical stresses in the as-prepared large-format cells and those caused by breathing strains in electrode active materials upon cycling [18,43–45]. However, the inclusion of even very small amounts of polymeric binders (e.g., 2 wt% or 5–7 vol%) in the composite electrodes leads to the area-specific resistances more than doubling and consequently to a significant degradation of capacity, which was attributed to the severe disruption of the Li^+ conduction pathways [17,18,39].

In our previous study, we demonstrated slurry-fabricable Li^+-conductive binders consisting of polymeric nitrile-butadiene rubber (NBR) and solvate ionic liquids (SILs, an equimolar complex of Li salt and glyme, denoted as Li(glyme)X, e.g., Li(G3)TFSI: G3 being triethylene glycol dimethyl ether and LiTFSI being lithium bis(trifluoromethanesulfonyl)imide) [18,36]. The SIL-based Li^+ conductive binders was processed using sulfide-compatible intermediately-polar solvents, such as dibromomethane (DBM). The SIL-based Li^+ conductive binders (NBR-Li(G3)TFSI: ~0.1 mS cm^{-1}) facilitated ionic contacts at the interfaces of the electrode active materials and the SEs, resulting in outstanding electrochemical performances at 30 °C.

Even with the opportunities promised by our previous results enabled by the inorganic–organic hybrid approach, a few critical concerns remained. First, despite the ionic liquid behavior of the SIL (Li(G3)TFSI), the introduction of the polar liquid components to sulfide materials may offset the thermal stability of an all-solid-state system: sulfide SE-SIL composites may decompose at elevated temperatures such as ~100 °C. Second, the application of the NBR-SILs to the graphite (Gr) anode has not yet been investigated. Third, DBM is too volatile and toxic as a processing solvent to be used for practical applications.

These considerations led us to examine the SIL-based Li^+-conductive binders under thermally abusive conditions and to the development of new liquid-free dry-polymer-electrolyte (DPE)-based Li^+-conductive binders that could also cope with practically adaptable processing solvents, such as benzyl acetate (BA). Significant improvements in utilizing electrode active materials and their outstanding thermal stability, enabled by the slurry-fabricable DPE-based binders, are demonstrated for both cathodes ($LiNi_{0.70}Co_{0.15}Mn_{0.15}O_2$ (NCM)) and anodes (Gr and $Li_4Ti_5O_{12}$ (LTO)) at 30 °C and 70 °C.

Results and discussion

For the reinvestigation of SIL-based binders, sheet-type NCM and Gr electrodes made of NBR with different SILs were prepared by the wet-slurry method using DBM. The electrodes consisted of the electrode active materials, $Li_6PS_5Cl_{0.5}Br_{0.5}$ (LPSX), Super C65, NBR, and SILs. The compositions of each SIL and electrode are provided respectively in Tables S2, S3. Fig. 1a (solid lines) shows the first-cycle charge–discharge voltage profiles at 0.1C (0.26 mA cm^{-2}) and 30 °C for the sheet-type NCM electrodes composed of Li^+-insulating binder (NBR) and Li^+-conductive SIL-type binders (NBR-Li(G3)TFSI and NBR-Li(G4)BETI: G4 is tetraethylene glycol dimethyl ether and LiBETI is lithium bis(pentafluoroethanesulfonyl)imide) in NCM/Li-In half cells. The use of NBR-SIL binders greatly improved the reversible capacity and initial Coulombic efficiency (ICE): From 144 mA h g^{-1} and 78.8%

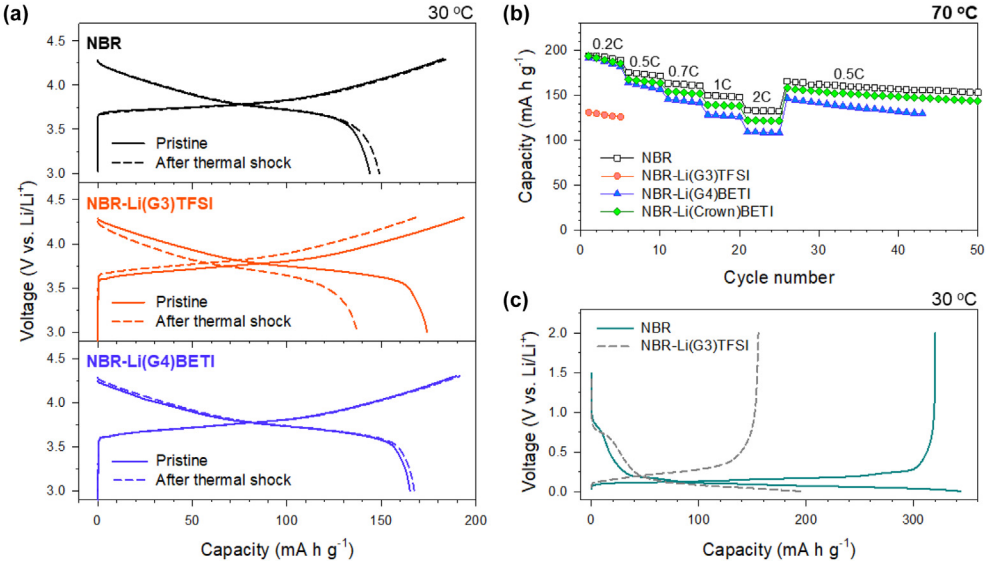

FIGURE 1

Results of NCM ($LiNi_{0.6}Co_{0.2}Mn_{0.2}O_2$ or $LiNi_{0.7}Co_{0.15}Mn_{0.15}O_2$) and Gr (graphite) electrodes in all-solid-state half cells employing the SIL (solvate ionic liquid)-based Li^+ conductive binders. (a) First-cycle charge–discharge voltage profiles at 30 °C without and with thermal shock (an exposure to 100 °C for 2 h) prior to cycling for NCM/Li-In all-solid-state cells employing NCM electrodes using conventional binder (NBR) and SIL-based Li^+-conductive binders of NBR-Li(G3)TFSI and NBR-Li(G4)BETI. (b) Rate capabilities at 70 °C for NCM/Li-In all-solid-state cells employing NCM electrodes using conventional binder (NBR) and SIL-based Li^+-conductive binders of NBR-Li(G3)TFSI, NBR-Li(G4)BETI, and NBR-Li(crown)BETI. (c) First-cycle charge–discharge voltage profiles at 30 °C for Gr/Li-In all-solid-state cells with Gr electrodes employing conventional binder NBR and SIL-based Li^+-conductive binder of NBR-Li(G3)TFSI.

for NBR to 174 mA h g^{-1} and 90.0% for NBR-Li(G3)TFSI and 165 mA h g^{-1} and 87.2% for NBR-Li(G4)BETI, which is consistent with our previous report [19].

To investigate their thermal stability, NCM electrodes were subjected to a thermal shock by storing them at 100 °C for 2 h prior to cycling at 30 °C (dashed lines in Fig. 1a). As compared with the result for using pristine NBR, the NCM electrodes with NBR-Li(G3)TFSI exhibited significantly degraded capacity and ICE (from 174 to 137 mA h g^{-1} and from 90.0 to 81.3%), indicating that the NBR-Li(G3)TFSI had lost its functionality and that a detrimental side reaction had occurred. Interestingly, the NCM electrodes made of another SIL-based binder NBR-Li(G4)BETI retained their performance after the thermal shock, which may be associated with complex interfacial evolution varied by the SILs' chemical environment [46,47].

The rate capabilities of the NCM electrodes with NBR and various NBR-SILs of NBR-Li(G3)TFSI, NBR-Li(G4)BETI, and NBR-Li (crown)BETI (crown: crown ether of 15-crown-5) in all-solid-state cells at a temperature of 70 °C are compared in Fig. 1b. In particular, the NCM with NBR-Li(G3)TFSI exhibited an even lower capacity of 131 mA h g^{-1} at 0.2C and 70 °C (Fig. 1b), when compared with the result at 30 °C (174 mA h g^{-1}, Fig. 1a). The use of the SIL consisting of bulkier anion (BETI rather than TFSI) and the glyme coordinating Li^+ ions more strongly (crown rather than glyme) resulted in improved performance (Li(G3)TFSI ≪ Li(G4)BETI < Li(crown)BETI) (Fig. 1b), indicating correspondingly attenuated thermal degradation [46]. Disappointingly, however, none of the results at 70 °C for the SIL-based binders outdid the performance for a simple NBR binder. It is also notable that the superior performance at 30 °C after the thermal shock for NCM

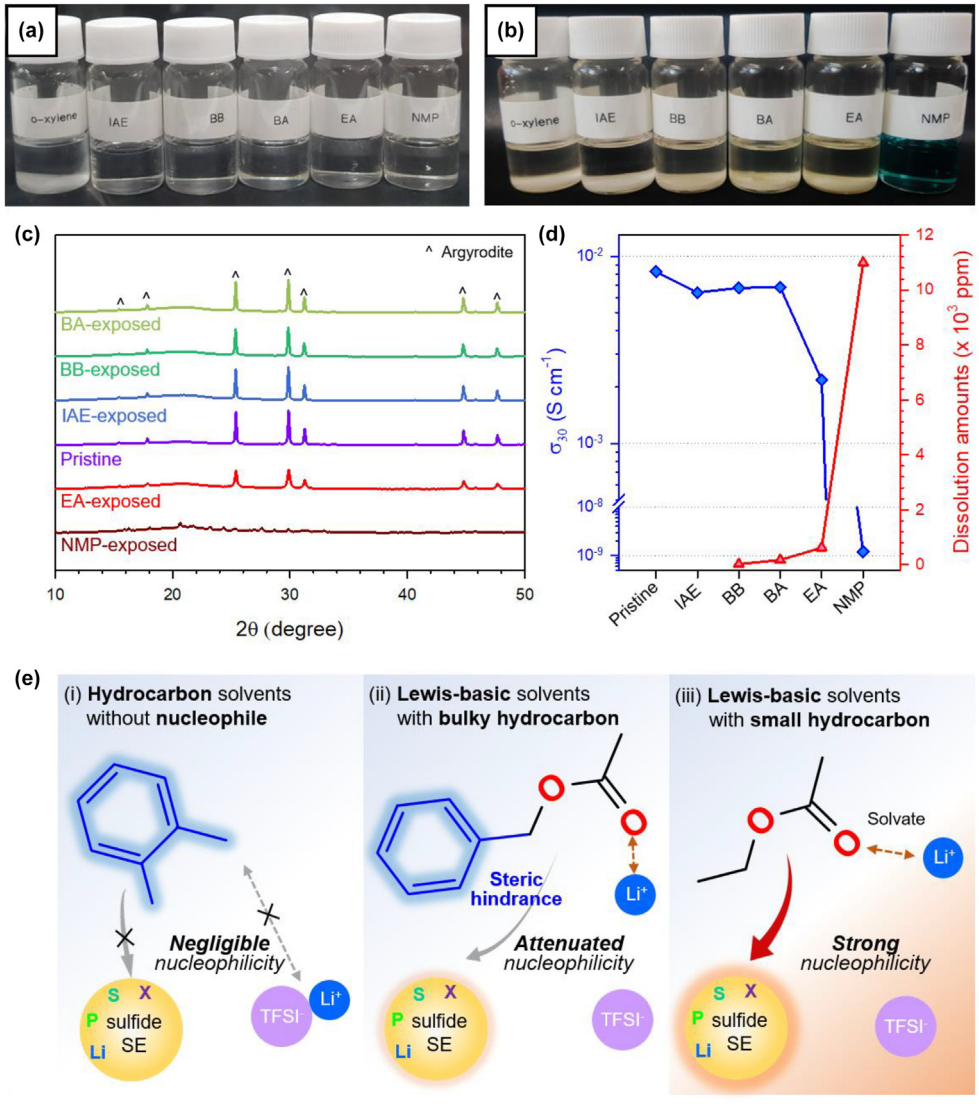

FIGURE 2

Compatibility results of slurry-processing solvents with sulfide SEs and Li salts, respectively. Photographs of (a) mixtures of LiTFSI and solvents, and (b) mixtures of LPSX and solvents. (c) XRD patterns of LPSX upon exposure to various solvents of NMP (N-methyl pyrrolidinone), EA (ethyl acetate), BA (benzyl acetate), BB (butyl butyrate), and IAE (isoamyl ether). (d) Li^+ conductivities at 30 °C and dissolved amounts for LPSX after the exposure to the solvents. (e) Schematic illustrating reactivity with LPSX for (i) hydrocarbon solvents (e.g., *o*-xylene), (ii) Lewis-basic solvents with bulky hydrocarbons (e.g., BA), and (iii) Lewis-basic solvents with small hydrocarbons (e.g., EA). Note that Lewis-basic solvents with bulky hydrocarbons, such as BA, does not react with LPSX due to the steric hindrance by the bulky benzyl group and can dissolve Li salts owing to the polar acetate group.

electrodes using NBR-Li(G4)BETI to those using NBR (Fig. 1a) did not hold for the results cycled at 70 °C (Fig. 1b). The SIL-related thermal deterioration at the interfaces could be accelerated by elevating the temperature. In short, the high-temperature physico/electrochemical stability of the three NBR-SILs in the proximity of the sulfide SEs and the NCM thus far, rank in ascending order Li(G3)TFSI ≪ Li(G4)BETI ≪ Li(crown)BETI. This is also consistent with the cyclic voltammetry results in a voltage range of 3.0–4.3 V (vs. Li/Li$^+$) at 70 °C (Fig. S1). The underlying mechanism could be closely linked to the steric effect and the affinity between the Li$^+$ and glyme in SILs [46,47], which is an intriguing subject for theoretical calculations such as those in molecular dynamics [5,48].

Another drawback of SILs is their poor compatibility with Gr anodes [49]. The first charge–discharge voltage profiles for Gr electrodes with and without Li(G3)TFSI in all-solid-state Gr/Li-In half-cells at 0.1C and 30 °C are shown in Fig. 1c. By employing NBR-Li(G3)TFSI, the reversible capacity drastically decreased from 320 to 126 mA h g^{-1}, when compared to the case without SILs (NBR). This result could be associated with sluggish interfacial charge-transfer kinetics and/or severe interfacial side reactions as evidenced by the noticeable sloping voltage plateau at 0.7–0.8 V (vs. Li/Li$^+$) during charge (lithiation) [49].

In summary of the results obtained; the presence of a liquid constituent such as glyme in the NBR-SILs facilitated the dissociation of Li salts and thus the mobility of Li$^+$ in the polymeric matrix, but it degraded thermal stability (Fig. 1a and b) and restricted applicability (Fig. 1c). DPEs without any small organic molecules, such as solvent molecules and plasticizers, could thus be considered as one of the most desirable candidates for troubleshooting the problems related with SILs.

A tactical approach is required to hybridize DPEs with sulfide SEs using the wet-slurry method. The processing solvents should act on both the Li salts and polymers while not being aggressive toward the vulnerable sulfide SEs. As a first step, comprehensive compatibility tests were conducted for LPSX and LiTFSI with var-

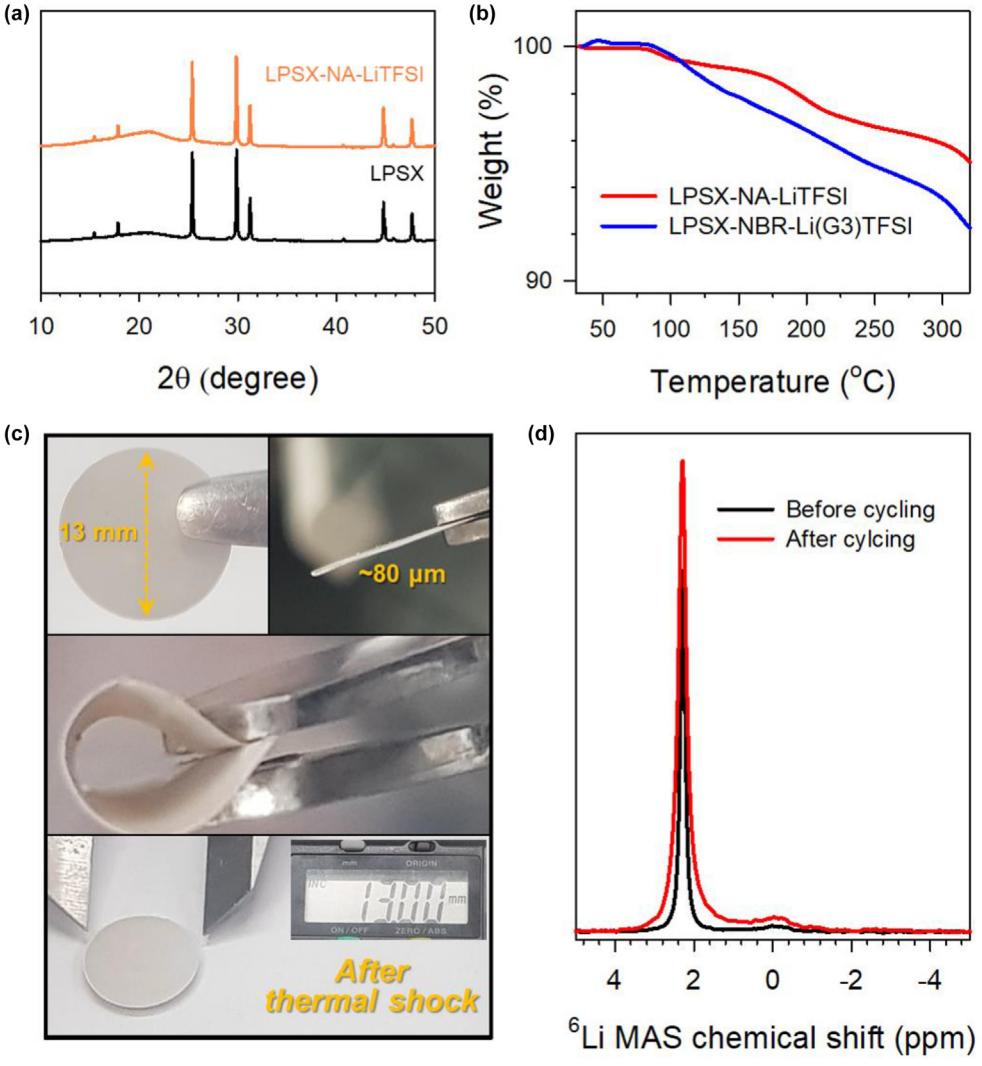

FIGURE 3

Characterization of LPSX-NA-LiTFSI composites. (a) XRD patterns of pristine LPSX and LPSX-NA-LiTFSI. (b) TGA profiles for SIL-type LPSX-NBR-Li(G3)TFSI and the liquid-free LPSX-NA-LiTFSI in Ar. (c) Photographs of thin LPSX-NA-LiTFSI membranes showing their flexibility and thermal stability (intact after thermal shock at 200 °C for 1 h). (d) MAS ^{6}Li NMR spectra of LPSX-NA-LiTFSI before and after cycling of ^{6}Li/(LPSX-NA-LiTFSI)/^{6}Li symmetric cells.

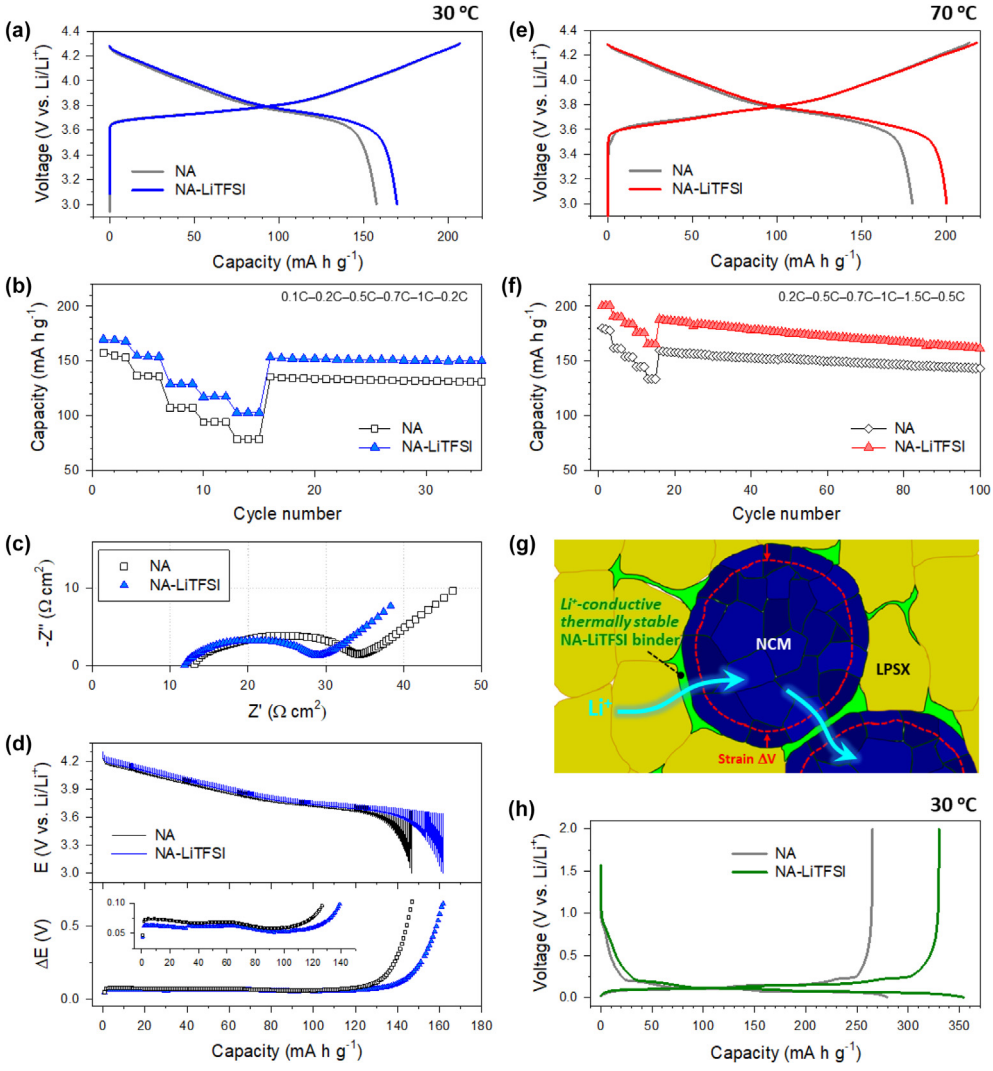

FIGURE 4

Electrochemical characterization of NCM and Gr in all-solid-state half cells, depending on the employment of the DPE-type binder (NA-LiTFSI) in the slurry-fabricated sheet-type electrodes. Results at 30 °C for (a) first-cycle charge–discharge voltage profiles at 0.1 C, (b) rate capabilities, (c) Nyquist plots, and (d) transient discharge voltage profiles and their corresponding polarization curves obtained by GITT for NCM electrodes made of binders without and with LiTFSI (NA and NA-LiTFSI, respectively). Results at 70 °C for (e) first-cycle charge–discharge voltage profiles at 0.2 C and (f) rate capabilities for NCM electrodes made of binders without and with LiTFSI. C-rates applied are shown in the panels of (b) and (f). (g) Schematic illustrating microstructure of NCM composite electrodes made of DPE-type binders, such as NA-LiTFSI, which provide unobstructed interfacial ionic transport pathways without thermal degradation despite volumetric strains of electrode active materials of NCM. (h) First-cycle charge–discharge voltage profiles at 0.1C and 30 °C for Gr electrodes made of binders without and with LiTFSI.

ious solvents (Fig. 2a and b). The detailed specifications for these solvents are provided in Table S4. Three types of solvents were selected: (i) hydrocarbon solvents (toluene, o-xylene), (ii) ester (R-COO-R′) or ether (R-O-R′)-based Lewis-basic solvents with varying alkyl groups (ethyl acetate (EA), benzyl acetate (BA), butyl butyrate (BB), and isoamyl ether (IAE)), and (iii) a strong Lewis-basic solvent NMP. The mixtures of hydrocarbon solvents (e.g., toluene and *o*-xylene) with LiTFSI or LPSX did not show any signs of reaction or dissolution. Importantly, LiTFSI could be fully dissolved into Lewis-basic solvents (e.g., EA, BA, BB, and IAE, and NMP) and LPSX was also partially eluted by them. In particular, the degrees of the dissolution of sulfide SEs into the Lewis-basic solvents appeared to differ among each other (Fig. 2b).

The chemical stability of LPSX against various Lewis-basic solvents was characterized by X-ray diffraction (XRD) measurements (Fig. 2c). After the LPSX powders were exposed to each solvent for 2 h, they were subjected to heat treatment at 150 °C under vacuum for drying. Interestingly, the Lewis-basic solvents with an identical functional group (i.e., ester group) resulted in different compatibilities with sulfide SEs. For the samples exposed to the Lewis-basic solvents bearing bulky hydrocarbons (e.g., IAE, BA, and BB), the characteristic argyrodite XRD peaks for LPSX remain unchanged without showing noticeable impurities (Fig. 2c). In stark contrast, LPSX exposed to EA bearing small hydrocarbons exhibited weakened and broadened peaks, indicating lowered crystallinity and in turn higher reactivity. For the case of exposure to NMP, unidentified XRD peaks emerged with

the disappearance of the argyrodite peaks, which is not surprising considering the strong Lewis-basicity of NMP.

Furthermore, for the Lewis-basic solvents, Li^+ conductivities, after the solvent-exposure, and the dissolution amounts into each solvent were measured using Li^+-blocking Ti/SE/Ti symmetric cells and inductively coupled plasma optical emission spectroscopy (ICPOES), respectively (Fig. 2d). The Li^+ conductivity trend was counter to the degree of dissolution, confirming the significance of the intactness of the solvents in reaction with sulfide SEs. Importantly, in consistence with the XRD results (Fig. 2c), a marginal degradation in Li^+ conductivity was obtained for the Lewis-basic solvents having bulky alkyl groups: pristine (8.3 mS cm^{-1}), BB-exposed (6.8 mS cm^{-1}), BA-exposed (6.8 mS cm^{-1}), and IAE-exposed (6.4 mS cm^{-1}). Owing to its non-toxicity (toxicity level: 1 vs. 2 for NMP) and adequate vapor pressure (0.177 mmHg vs. 0.370 mmHg for NMP) (Table S3), BA is the most appropriate solvent for a wet-slurry process using DPE-based binders. Moreover, BA dissolves numerous polymer candidates for DPEs (Table S5).

Fig. 2e contains the comprehensive explication of the aforementioned compatibility test results. The hydrocarbon solvents with negligible donor ability such as o-xylene are inert to LPSX and LiTFSI because a polar functional group is absent (case i). In contrast, solvents containing Lewis-basic functional groups (e.g., ethers and esters) have an inherent ability to dissolve LiTFSI and LPSX. However, reactivities of the same ester-based Lewis-basic solvents for sulfide SEs varied among each other (Fig. 2b–d), which could be explained by the steric effect in organic chemistry. With EA having a short alkyl chain (e.g., EA, case iii), considerable dissolution of LPSX is inevitable by nucleophilic attack from the ester group having lone-pair electrons at electronegative oxygen. In contrast, the substitution of the ethyl group in EA with a bulky benzyl group (BA, case ii) could significantly attenuate nucleophilic attack, resulting in excellent compatibility with sulfide SEs (Fig. 2b–d) while retaining its dissolving power toward LiTFSI (Fig. 2a).

Thanks to the versatility of BA, various polymer-LPSX composites could be fabricated by a wet-slurry protocol. The intactness of the characteristic argyrodite XRD peaks was confirmed for the LPSX-polymer composites prepared from the BA-based wet-slurry aged for up to 3 days (Fig. S2). The corresponding Li^+ conductivities also remained unchanged after storage for 2 days at 30 °C (Table S6). Unfortunately, only NBR showed relatively good adhesion (Fig. S3) among the NCM electrodes prepared using various polymer candidates via the BA-based slurry-process. Thus, other polymer candidates were blended with NBR for sheet-type electrodes. The electrodes employing NBR-blended polymers showed mechanically compliant properties.

For the assessment of DPE-based Li^+-conductive binders, a composite of LPSX, NBR, poly(1,4-butylene adipate), and LiTFSI (denoted as LPSX-NA-LiTFSI) was selected as a model system. The LPSX-NA-LiTFSI processed using BA tolerated a high-temperature drying process at 150 °C, as confirmed by the XRD data (Fig. 3a). Thermogravimetric analysis (TGA) results for the composite using SIL-based Li^+-conductive binder (LPSX-NBR-Li(G3)TFSI) and the one using DPE-based Li^+-conductive binder (LPSX-NA-LiTFSI) are compared in Fig. 3b. While significant weight loss started at <100 °C for the case using SIL-based binder, the use of DPE-based binder resulted in much better weight retention up to ~170 °C. This result confirms the excellent thermal stability of the DPE-based binder, which agrees with the electrochemical results in Fig. 1a-c. In addition, LPSX-NA-LiTFSI could be fabricated as 80 μm thick flexible SE films (Fig. 3c). Furthermore, the composite SE films did not suffer from any thermal shrinkage after exposure at 200 °C (Fig. 3c). These results unambiguously confirm the outstanding thermal stability which ensures excellent safety parameters for the resulting ASLBs.

The Li^+ conductivity contour plot at 30 °C obtained for various ternary compositions for LPSX-NA-LiTFSI is depicted in Fig. S4. The improvement in Li^+ conductivity by introducing LiTFSI was not significant at the optimal compositions; 1.9 mS cm^{-1} for LPSX-NA (97:3 wt. ratio) and 2.2 mS cm^{-1} for LPSX-NA-LiTFSI (96.5:3.0:0.5 wt. ratio), which is due to the much lower conductivity of NA-LiTFSI (10^{-7}-10^{-6} S cm^{-1}) compared to that of LPSX (8.3 mS cm^{-1}). Nevertheless, the introduction of LiTFSI is still meaningful as it could render the polymeric binder domains Li^+-conductive [18,44]. The ^6Li magic angle spinning (MAS) nuclear magnetic resonance (NMR) experiments were performed for the LPSX-NA-LiTFSI collected from the ^6Li/LPSX-NA-LiTFSI/^6Li symmetric cells (Fig. 3d). After repeated cycling, the intensity increased not only for the Li in LPSX at 2.28 ppm but

TABLE 1

Electrochemical performances of electrodes in all-solid-state half cells.

Electrode	Temperature	Binder	Initial capacity (mA h g^{-1})		ICE (%)
			Charge	Discharge	
NCM ($LiNi_{0.70}Co_{0.15}Mn_{0.15}O_2$)	30 °C	NA	206	158	76.4
		NA-TFSI	207	170	81.9
	70 °C	NA	214	180	84.2
		NA-TFSI	218	200	91.8
Gr[a]	30 °C	NA	280	265	94.7
		NA-TFSI	354	330	93.2
LTO[a]	30 °C	NA	88	77	87.7
		NA-TFSI	97	85	87.5

[a] Despite the tests using half cells, lithiation and de-lithiation capacities are assigned to the charge and discharge capacities, respectively.

also for the Li in the NA-LiTFSI at −0.02 ppm, confirming that the Li^+ transport is facilitated by the DPE-based binders [18,50].

The electrochemical performances of sheet-type electrodes for NCM and Gr, prepared by tailoring the DPE-type Li^+-conductive binder (NA-LiTFSI) via the wet-slurry process using BA, in half cells are shown in Fig. 4 and summarized in Table 1. Cross-sectional field emission scanning electron microscopy (FESEM) images for the electrodes are shown in Fig. S5. Detailed specifications for these electrodes are provided in Table S7. The first charge–discharge voltage profiles for NCM without and with LiTFSI at 0.1C (0.27 mA cm^{-2}) and 30 °C are shown in Fig. 4a. The NCM electrodes with LiTFSI showed a discharge capacity of 170 mA h g^{-1}, outperforming the one without LiTFSI (158 mA h g^{-1}), which is also consistent with the corresponding rate capability results (Fig. 4b). Moreover, the ICE increased from 76.4% (without LiTFSI) to 82.1% (with LiTFSI), which is discussed later. It is shown that the use of LiTFSI in NA resulted in the interfacial resistance decreasing from 20 to 16 Ω cm^2 in the Nyquist plots (Fig. 4c) and the lowered polarization in the galvanostatic intermittent titration technique (GITT) results (Fig. 4d).

Thermally abusive testing at 70 °C was also applied (Fig. 4e and f). The NCM electrodes made of binders having LiTFSI exhibited a remarkable performance: the reversible capacity of 200 mA h g^{-1} and ICE of 91.7%, is a significant improvement, compared to the case of using the conventional Li^+-insulating binder NA (180 mA h g^{-1} and 84.2%). Importantly, this achievement is in stark contrast to the result of using NBR-SIL (131 mA h g^{-1} and 78.9%, Fig. 1b), which highlights the excellent thermal stability of the DPE-based binder, in agreement with the results for TGA (Fig. 3b) and CV (Figs. S1 and S6). The discharge capacities at 70 °C for the NCM electrodes, varied by C-rates, as a function of cycle number are also shown in Fig. 4f. The kinetics was boosted at 70 °C and NCM electrodes made of NA-LiTFSI showed 26% higher capacity at 1.5C (166 mA h g^{-1}), as compared to those made of NA without LiTFSI (132 mA h g^{-1}). The NCM electrodes with NA-LiTFSI show an acceptable capacity retention of 86% after 100 cycles, as compared to their capacity at the 16th cycle. A comparative experiment also confirmed that ASLBs with LPSX-NA-LiTFSI showed much superior high-temperature (70 °C) durability, compared to liquid electrolyte cells (Fig. S7). The NCM electrodes tested at low temperatures of 0 and −10 °C showed large overpotential and thus lowered capacities (Fig. S8). Interestingly, at these low temperatures, the NCM electrodes made of NA-LiTFSI showed comparable or slightly higher capacities, as compared to those made of NA without using LiTFSI, which confirms the wider temperature operability of the DPE-type-binder-based electrodes. Furthermore, NCM electrodes tailored by using DPE-binders made of different polymers, such as poly(vinyl acetate) (PVA) and poly(propylene carbonate) (PPC), were tested at 30 °C (Fig. S9). Consistently with the results for using NA-LiTFSI, the NCM electrodes composed of a variety of DPE-binders also produced similarly improved capacities, when compared to those binders without LiTFSI. This highlights the generalized application for ASLB slurry and the potential for extensive development further. In short, the developed DPE-binders provide unobstructed Li^+ transport pathways with thermal and mechanical stability, as illustrated in Fig. 4g.

The enhancement of electrochemical performance by the application of DPE-binder was also effective for other types of electrodes. Gr electrodes consisting of NA-LiTFSI showed a 65 mA h g^{-1} improvement in discharge capacity (from 265 to 330 mA h g^{-1} at 0.1C and 30 °C) when compared to those made of NA (Fig. 4h). This result is in sharp contrast to that for employing NBR-SIL (from 320 to 126 mA h g^{-1} Fig. 1c). (Note that the difference in capacity for reference Gr electrodes in Fig. 4h (265 mA h g^{-1}) and Fig. 1c (320 mA h g^{-1}) is due to the different weight fractions of SE in the electrodes made of NA-LiTFSI and NBR-Li(G3)TFSI: 33.5 and 47.5 wt%, respectively). LTO also showed a capacity improvement with the application of NA-LiTFSI (Fig. S10).

Interestingly, it is notable that the improvements in ICE by the application of NA-LiTFSI varied by electrodes (Table 1); significantly for NCM from 76.4 to 81.9% but not for Gr (from 94.7 to 93.2%) or LTO (from 87.7 to 87.5%). Several factors may have caused this result. Li^+-conductive binders could effectively mitigate the occurrence of electrochemo-mechanical failure. NCM suffers from ionic contact loosening/losses not only at the SE-NCM interfaces but also in the disintegrated secondary particles, both of which are responsible for lowering ICEs [51,52]. In contrast, the zero-strain LTO is free from any electrochemo-

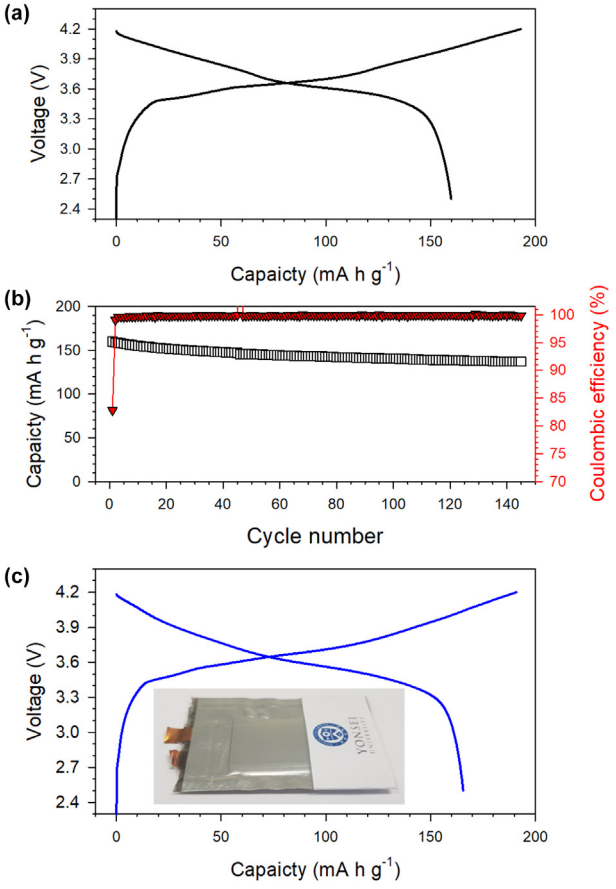

FIGURE 5

Results of NCM/Gr all-solid-state full cells at 30 °C. (a) First-cycle charge–discharge voltage profiles and (b) cycling performance for pelletized full cells. (c) First-cycle charge–discharge voltage profiles for 16 × 25 mm^2 pouch-type full cells.

mechanical degradation. Even though the volumetric strain for Gr is the highest (~13%) [53], Gr maintains acceptable electrical conductivity within itself upon cycling and does not disintegrate. For NCM, the DPE-binders may infiltrate into any void spaces formed by the disintegration of secondary particles and mitigate electrochemo-mechanical degradation. This may be supported by the presence of F^- signals in the NCM domains from time-of-flight secondary ion mass spectrometry (TOFSIMS) results (Fig. S11). Considering that the highly unstable interfacial feature between NCM and sulfide SEs contributes to the lowering of ICEs [51,52,54–56], the possibility of alleviated interfacial side reactions by the occupation of DPEs at the interfaces could also not be ruled out [18,27]. These scenarios need to be investigated in future work.

Finally, all-solid-state NCM/Gr full cells with sheet-type electrodes tailored by the wet-slurry method using the DPE-binder NA-LiTFSI were tested in the voltage range of 2.5–4.2 V at 30 °C (Fig. 5). Two types of full cells, pelletized cells, and 16×25 mm^2 pouch-type cells were assembled. Thin LSPX-NA-LiTFSI films (70–80 μm) were used between the cathode and anode as a separator layer. The full cells showed similarly high reversible capacities of 160 at 0.1C and 166 mA h g^{-1} at 0.05C for the pelletized and pouch cells, respectively, which is consistent with the estimations from the half-cell results. The interfacial resistance of NCM/Gr full cells was ~48 Ω cm^2 (Fig. S12). Cycling retention for the pelletized full cells after 145 cycles was 85.7% (Fig. 5b).

The current status of slurry-fabricated sheet-type electrodes for ASLBs is depicted in Fig. S13 (detailed information is listed in Table S8). Sheet-type electrodes fabricated using oxide or DPEs exhibited insufficiently high areal capacity even at lower current density and high operating temperature (>50 °C), which is owing to their low Li^+ conductivities. In this work using sulfide SEs, sheet-type electrodes tailored using NA-LiTFSI and versatile BA exhibited higher capacity and wider-temperature operability (up to 70 °C) with higher mass loading, compared with those of sheet-type electrodes fabricated using conventional binders (e.g., NBR) and volatile solvents (e.g., toluene, xylene).

Conclusions

In summary, a new tactical hybridization protocol for slurry-fabricable Li^+-conductive DPE-type binders with high thermal stability was developed for ASLBs. The ester solvents bearing bulky alkyl groups, such as BA (benzyl acetate), as the slurry solvent are practically adaptable (nontoxic and with appropriate vapor pressure) and enabled the dissolution of both polymers and Li salts while remaining intact when in contact with vulnerable sulfide SEs. Flexible SE films and sheet-type electrodes with excellent thermal stability were fabricated according to the wet-slurry method using BA and DPE-type binders. The employment of DPE-type binders, such as NA-LiTFSI, significantly improved the utilization of electrode active materials for NCM (from 158 to 170 mA h g^{-1}) and Gr (from 265 to 320 mA h g^{-1}). Moreover, the DPE-type binders retained their functionality during 70 °C high-temperature testing conditions. These results are in contrast with the poor electrochemical performance of all-solid-state cells employing SIL-type binders (e.g., NBR-Li(G3)TFSI) for Gr electrodes or those tested under thermally abusive conditions (thermal shock prior to testing or testing at 70 °C). Moreover, the feasibility for DPE-binders composed of polymers, such as PVA and PPC, was also confirmed, thus highlighting wide range of applicability for the developed protocol. Finally, NCM/Gr all-solid-state full cells employing electrodes and SE films made of NA-LiTFSI demonstrated promising performance. We believe that our results shed light on a design strategy for hybridizing materials and marks a breakthrough in the development of practical all-solid-state technologies.

Experimental

Preparation of materials

For the LPSX ($Li_6PS_5Cl_{0.5}Br_{0.5}$), a stoichiometric mixture of Li_2S (99.9%, Alfa Aesar), P_2S_5 (99%, Sigma Aldrich), LiCl (99.99%, Sigma Aldrich), and LiBr (99.9%, Alfa Aesar) was mechanically ball-milled at 600 rpm for 10 h in a ZrO_2 vial with ZrO_2 balls using Pulverisette 7PL (Fritsch GmbH). The resulting powders were annealed at 550 °C for 5 h. Wet-chemical coatings of $LiNbO_3$ on NCM ($LiNi_{0.6}Co_{0.2}Mn_{0.2}O_2$ and $LiNi_{0.7}Co_{0.15}Mn_{0.15}O_2$) powders (0.5 wt%) were carried out using lithium ethoxide (95%, Sigma Aldrich), niobium ethoxide (99.95%, Sigma Aldrich), and anhydrous ethanol (99.9%, Sigma Aldrich) by following a procedure in our previous work.[19] For the preparation of SILs, equimolar mixture of glymes (G3 (99%, Sigma Aldrich) or G4 (≥99%, Sigma Aldrich) or 15-crown-5 (98%, Sigma Aldrich)) and Li salts (LiTFSI (lithium bis(trifluoromethane)sulfonamide, 99.95%, Sigma Aldrich) or LiBETI (lithium bis(pentafluoroethane sulfonyl)imide, 98%, TCI Corp.)) were mixed overnight at 60 °C. The LPSX-Polymers-LiTFSI and LPSX-NBR-SILs were prepared by the wet-slurry method using benzyl acetate (BA, 99%, Sigma Aldrich) and dibromomethane (DBM, 99%, Sigma Aldrich), respectively. The slurries were dried at 150 °C for the LPSX-Polymers-LiTFSI and 60 °C for LPSX-NBR-SILs. NBR (37–39 wt. % of nitrile contents), poly(1,4-butylene adipate), PPC, PVA, and poly(epichlorohydrin) were purchased from Sigma Aldrich. All processes were conducted in the Ar-filled glove box.

Fabrication of electrodes

The wet-slurries made of active materials, binders, super C65, Li salts (or SILs), and BA (or DBM) were prepared by mixing targeted composition and coated on the Al (or Ni) foil by doctor-blade method with the doctor blade gap height of 280 μm. The slurry-coated electrodes were then dried at 150 or 60 °C under vacuum. For NCM electrodes with and without SILs, solid contents were adjusted ~49 and 72 wt.%, respectively. For the SE layers, LPSX-NA or LPSX-NA-LiTFSI were prepared by mixing targeted composition in BA with solid content of ~53 wt.%.

Material characterization

For the XRD measurements, the samples were sealed with a beryllium window and mounted on a MiniFlex 600 diffractometer (Rigaku Corp., Cu Kα radiation of 1.5406 Å) and measured at 40 kV and 15 mA. The TGA data were recorded ranging from room temperature to 350 °C at 5 °C min^{-1} under Ar using a Q50 (TA Instrument Corp.). To assess the reactivity between LPSX and various solvents, 100 mg of LPSX were stored in 10 mL of each solvent. After they were kept for 2 h, the digital

images were taken. Afterwards, supernatants were collected by syringe-type filtration and subjected to the measurements via ICPOES using 720-ES (Varian). For the ^{6}Li NMR experiments, ^{6}Li/(LPSX-NA-LiTFSI)/^{6}Li symmetric cells were charged and discharged continuously at a constant current of 50 μA and 70 °C. The LPSX-NA-LiTFSI samples collected before and after cycling were subjected to the ^{6}Li NMR measurements using AVANCE III 40 (Bruker). The obtained NMR intensities were normalized by the sample weight. The spinning rate for MAS ^{6}Li NMR measurements was 10 kHz. For the cross-sectional FESEM measurements, electrode samples were polished with an Ar ion beam initially at 6 kV for 6 h and then at 4 kV for 3 h (JEOL, IB19510CP). FESEM images were obtained using AURIGA (Zeiss). To avoid any air exposure of the polished samples, an air-tight transfer box, DME 2830 (SEMILAB), was used.

Electrochemical characterization

The Li–In counter electrodes ($Li_{0.5}In$: LPSX = 8:2 wt. ratio) were prepared by ball-milling In (Aldrich, 99%), Li (FMC Lithium Corp.), and LPSX powders. 150 mg of LPSX was pelletized under 100 MPa to form SE layers (~600 μm). Then, the as-prepared sheet-type electrodes (NCM, Gr, LTO) and Li–In electrode were placed on each side of the SE layer. Finally, the all-solid-state NCM (or Gr, LTO)/Li-In half cells were fabricated by pelletizing at 370 MPa. For the pellet-type and pouch-type NCM/Gr full cells, thin LSPX-NA-LiTFSI films (70–80 μm) were used. The areal capacity ratio of negative to positive electrodes (np ratio) was 1.16 for the pelletized cell and 1.25 for the pouch cell, respectively. The pelletized and pouch-type cells were tested under an external pressure of ~70 and ~2 MPa, respectively. The EIS data were recorded with an amplitude of 10 mV and a frequency range from 10 mHz to 1 MHz using a VMP3 (Bio-Logic). For the EIS measurements, the cells were charged to 4.3 V (vs Li/Li$^+$) at 0.1C at the first cycle, followed by rest for 3 h. The GITT measurements were carried out with a pulse current of 0.5 C for 60 s and rest for 2 h. For tracking the Li$^+$ pathways, ^{6}Li$^+$-ion non-blocking symmetric cells were made as described in our previous report.

CRediT authorship contribution statement

Dae Yang Oh: Conceptualization, Methodology, Investigation, Writing - original draft. **Kyu Tae Kim:** Methodology, Investigation. **Sung Hoo Jung:** Investigation. **Dong Hyeon Kim:** Investigation. **Seunggoo Jun:** Investigation. **Sungeun Jeoung:** Data curation. **Hoi Ri Moon:** Formal analysis. **Yoon Seok Jung:** Conceptualization, Supervision, Writing - review & editing.

Declaration of Competing Interest

The authors declare that they have no known competing financial interests or personal relationships that could have appeared to influence the work reported in this paper.

Acknowledgements

D. Y. Oh and K. T. Kim contributed equally to this work. This work was supported by Hyundai Motors, by the Technology Development Program to Solve Climate Changes and by the Basic Science Research Program through the National Research Foundation of Korea (NRF) funded by the Ministry of Science, ICT & Future Planning (NRF2017M1A2A2044501 and NRF-2018R1A2B6004996), and by the Technology Innovation Program (20007045) funded By the Ministry of Trade, Industry & Energy (MOTIE, Korea), and by the Yonsei University Research Fund of 2020 (2020-22-0531).

Appendix A. Supplementary data

Supplementary data to this article can be found online at https://doi.org/10.1016/j.mattod.2021.01.006.

References

[1] Y. Kato et al., Nat. Energy 1 (2016) 16030.
[2] J. Janek, W.G. Zeier, Nat. Energy 1 (2016) 16141.
[3] X. Han et al., Nat. Mater. 16 (2017) 572–579.
[4] A. Manthiram, X. Yu, S. Wang, Nat. Rev. Mater. 2 (2017) 16103.
[5] K.H. Park et al., Adv. Energy Mater. 8 (2018) 1800035.
[6] Z. Zhang et al., Energy Environ. Sci. 11 (2018) 1945–1976.
[7] K. Liu et al., Sci. Adv. 4 (2018) eaas9820.
[8] T. Asano et al., Adv. Mater. 30 (2018) 1803075.
[9] F. Han et al., Nat. Energy 4 (2019) 187–196.
[10] M.J. Wang, R. Choudhury, J. Sakamoto, Joule 3 (2019) 2165–2178.
[11] S. Kim et al., Nat. Commun. 10 (2019) 1081.
[12] R. Chen et al., Chem. Rev. (2019) 6820–6877.
[13] L. Duchêne et al., Energy Storage Mater. 25 (2020) 782–794.
[14] R. Malik, Joule 2 (2018) 377–378.
[15] A.-Y. Song et al., Adv. Energy Mater. 10 (2020) 1903480.
[16] A. Aboulaich et al., Adv. Energy Mater. 1 (2011) 179–183.
[17] A. Sakuda, A. Hayashi, M. Tatsumisago, Sci. Rep. 3 (2013) 2261.
[18] Y.J. Nam et al., J. Power Sources 375 (2018) 93–101.
[19] D.Y. Oh et al., Adv. Energy Mater. 9 (2019) 1802927.
[20] Y. Liu et al., J. Power Sources 393 (2018) 193–203.
[21] Q. Zhang et al., Adv. Mater. 31 (2019) 1901131.
[22] H.-J. Deiseroth et al., Angew. Chem. Int. Ed. 47 (2008) 755–758.
[23] P. Adeli et al., Angew. Chem. Int. Ed. 58 (2019) 8681–8686.
[24] M. Li et al., Chem. Rev. (2020) 6783–6819.
[25] T. Inada et al., Solid State Ion. 158 (2003) 275–280.
[26] S. Ito et al., J. Power Sources 248 (2014) 943–950.
[27] J.M. Whiteley et al., Adv. Mater. 27 (2015) 6922–6927.
[28] Y.J. Nam et al., Nano Lett. 15 (2015) 3317–3323.
[29] D.H. Kim et al., Nano Lett. 17 (2017) 3013–3020.
[30] D.Y. Oh et al., J. Mater. Chem. A 5 (2017) 20771–20779.
[31] N. Riphaus et al., J. Electrochem. Soc. 165 (2018) A3993–A3999.
[32] S. Yu et al., J. Mater. Chem. A 6 (2018) 18304–18317.
[33] X. Chi et al., Angew. Chem. Int. Ed. Engl. 57 (2018) 2630–2634.
[34] D.H. Kim et al., ACS Energy Lett. 5 (2020) 718–727.
[35] G. Sahu et al., Energy Environ. Sci. 7 (2014) 1053–1058.
[36] S.-L. Shang et al., ACS Appl. Mater. Interfaces 9 (2017) 16261–16269.
[37] D.Y. Oh et al., Adv. Energy Mater. 5 (2015) 1500865.
[38] K. Lee et al., J. Electrochem. Soc. 164 (2017) A2075–A2081.
[39] T. Ates et al., Energy Storage Mater. 17 (2019) 204–210.
[40] D.H.S. Tan et al., ACS Appl. Energy Mater. 2 (2019) 6542–6550.
[41] F. Hippauf et al., Energy Storage Mater. 21 (2019) 390–398.
[42] Y.-G. Lee et al., Nat. Energy (2020) 299–308.
[43] Y.J. Nam et al., J. Mater. Chem. A 6 (2018) 14867–14875.
[44] J. Schnell et al., J. Power Sources 382 (2018) 160–175.
[45] A. Bielefeld, D.A. Weber, J. Janek, ACS Appl. Mater. Interfaces 12 (2020) 12821–12833.
[46] S. Tsuzuki et al., ChemPhysChem 14 (2013) 1993–2001.
[47] C. Zhang et al., J. Phys. Chem. B 118 (2014) 5144–5153.
[48] K. Shimizu et al., Phys. Chem. Chem. Phys. 17 (2015) 22321–22335.
[49] H. Moon et al., J. Phys. Chem. C 118 (2014) 20246–20256.
[50] J. Zheng, M. Tang, Y.-Y. Hu, Angew. Chem. Int. Ed. 55 (2016) 12538–12542.
[51] S.H. Jung et al., Adv. Energy Mater. 10 (2020) 1903360.
[52] R. Koerver et al., Chem. Mater. 29 (2017) 5574–5582.
[53] Y. Koyama et al., Adv. Funct. Mater. 16 (2006) 492–498.
[54] S.H. Jung et al., Chem. Mater. 30 (2018) 8190–8200.
[55] X. Li et al., Energy Environ. Sci. (2020) 1429–1461.
[56] Y. Xiao et al., Nat. Rev. Mater. 5 (2020) 105–126.